Science AAAS

pole, then α would be the co-latitude of the struts and the longitudinal angle between the struts would be 120°.

16. The presence of the factor of c^2 confirms that this is a relativistic effect. There is no swimming effect in the analogous Newtonian problem.

17. The fact that the swimming displacement per stroke is so small means that, strictly speaking, one should consider the swimming effect relative to the ordinary nonswimming geodesic motion of the

swimmer. However, the calculation that is presented is enough to show the existence of the effect that is surely also present in more complicated situations. Perhaps the most interesting case to consider would be a swimmer in a circular orbit, where the swimming effect could be used to gradually increase the radius of the orbit.

18. I thank J. Touma for infecting me with his interest in geometric phase and for bringing the articles of A. Shapere and F. Wilczek to my atten-

REPORTS

Coherent Quantum Dynamics of a Superconducting Flux Qubit

I. Chiorescu,[1]* Y. Nakamura,[1,2] C. J. P. M. Harmans,[1] J. E. Mooij[1]

We have observed coherent time evolution between two quantum states of a superconducting flux qubit comprising three Josephson junctions in a loop. The superposition of the two states carrying opposite macroscopic persistent currents is manipulated by resonant microwave pulses. Readout by means of switching-event measurement with an attached superconducting quantum interference device revealed quantum-state oscillations with high fidelity. Under strong microwave driving, it was possible to induce hundreds of coherent oscillations. Pulsed operations on this first sample yielded a relaxation time of 900 nanoseconds and a free-induction dephasing time of 20 nanoseconds. These results are promising for future solid-state quantum computing.

It is becoming clear that artificially fabricated solid-state devices of macroscopic size may, under certain conditions, behave as single quantum particles. We report on the controlled time-dependent quantum dynamics between two states of a micron-size superconducting ring containing billions of Cooper pairs (1). From a ground state in which all the Cooper pairs circulate in one direction, application of resonant microwave pulses can excite the system to a state where all pairs move oppositely, and make it oscillate coherently between these two states. Moreover, multiple pulses can be used to create quantum operation sequences. This is of strong fundamental interest because it allows experimental studies on decoherence mechanisms of the quantum behavior of a macroscopic-sized object. In addition, it is of great importance in the context of quantum computing (2) because these fabricated structures are attractive for a design that can be scaled up to large numbers of quantum bits or qubits (3).

Superconducting circuits with mesoscopic Josephson junctions are expected to behave according to the laws of quantum mechanics if they are separated sufficiently from external degrees of

freedom, thereby reducing the decoherence. Quantum oscillations of a superconducting two-level system have been observed in the Cooper pair box qubit using the charge degree of freedom (4). An improved version of the Cooper pair box qubit showed that quantum oscillations with a high quality factor could be achieved (5). In addition, a qubit based on the phase degree of freedom in a Josephson junction was presented, consisting of a single, relatively large Josephson junction current-biased close to its critical current (6, 7).

Our flux qubit consists of three Josephson junctions arranged in a superconducting loop threaded by an externally applied magnetic flux near half a superconducting flux quantum $\Phi_0 = h/2e$ [(8); a one-junction flux qubit is described in (9)]. Varying the flux bias controls the energy level separation of this effectively two-level system. At half a flux quantum, the two lowest states are symmetric and antisymmetric superpositions of two classical states with clockwise and anticlockwise circulating currents. As shown by previous microwave spectroscopy studies, the qubit can be engineered such that the two lowest eigenstates are energetically well separated from the higher ones (10). Because the qubit is primarily biased by magnetic flux, it is relatively insensitive to the charge noise that is abundantly present in circuits of this kind.

The central part of the circuit, fabricated by electron beam lithography and shadow

evaporation of Al, shows the three in-line Josephson junctions together with the small loop defining the qubit in which the persistent current can flow in two directions, as shown by arrows (Fig. 1A). The area of the middle junction of the qubit is $\alpha = 0.8$ times the area of the two outer ones. This ratio, together with the charging energy $E_C = e^2/2C$ and the Josephson energy $E_J = hI_C/4\pi e$ of the outer junctions (where I_C and C are their critical current and capacitance, respectively), determines the qubit energy levels (Fig. 2A) as a function of the superconductor phase γ_q across the junctions (Fig. 1B). Close to $\gamma_q =$
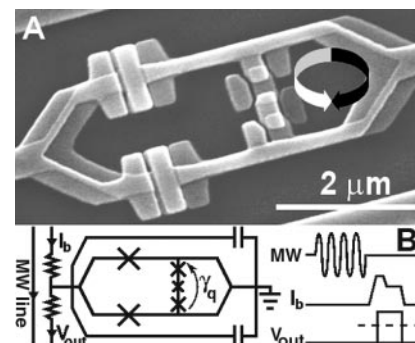

Fig. 1. (**A**) Scanning electron micrograph of a flux qubit (small loop with three Josephson junctions of critical current ~0.5 μA) and the attached SQUID (large loop with two big Josephson junctions of critical current ~2.2 μA). Evaporating Al from two different angles with an oxidation process between them gives the small overlapping regions (the Josephson junctions). The middle junction of the qubit is 0.8 times the area of the other two, and the ratio of qubit/SQUID areas is about 1:3. Arrows indicate the two directions of the persistent current in the qubit. The mutual qubit/SQUID inductance is $M \approx 9$ pH. (**B**) Schematic of the on-chip circuit; crosses represent the Josephson junctions. The SQUID is shunted by two capacitors (~5 pF each) to reduce the SQUID plasma frequency and biased through a resistor (~150 ohms) to avoid parasitic resonances in the leads. Symmetry of the circuit is introduced to suppress excitation of the SQUID from the qubit-control pulses. The MW line provides microwave current bursts inducing oscillating magnetic fields in the qubit loop. The current line provides the measuring pulse I_b and the voltage line allows the readout of the switching pulse V_{out}. The V_{out} signal is amplified, and a threshold discriminator (dashed line) detects the switching event at room temperature.

[1]Quantum Transport Group, Department of NanoScience, Delft University of Technology and Delft Institute for Micro Electronics and Submicron Technology (DIMES), Lorentzweg 1, 2628 CJ Delft, Netherlands. [2]NEC Fundamental Research Laboratories, 34 Miyukigaoka, Tsukuba, Ibaraki 305-8501, Japan.

*To whom correspondence should be addressed. E-mail: chiorescu@qt.tn.tudelft.nl

π, the loop behaves as a two-level system with an energy separation $E_{10} = E_1 - E_0$ of the eigenstates $|0\rangle$ and $|1\rangle$ described by the effective Hamiltonian $H = -\varepsilon\sigma_z/2 - \Delta\sigma_x/2$, where $\sigma_{z,x}$ are the Pauli spin matrices, Δ is the level repulsion, and $\varepsilon \approx I_p\Phi_0(\gamma_q - \pi)/\pi$ (where $I_p \approx 2\pi\alpha E_J/\Phi_0$ is the qubit maximum persistent current) (11).

The sample is enclosed in a gold-plated copper shielding box kept at cryogenic temperatures $T = 25$ mK ($k_B T \ll \Delta$). The qubit is initialized to the ground state simply by allowing it to relax. Coherent control of the qubit state is achieved by applying resonant microwave excitations on the microwave (MW) line (Fig. 1B), thereby inducing an oscillating magnetic field through the qubit loop. The qubit state evolves driven by a time-dependent term $(-\frac{1}{2})\varepsilon_{mw}\cos(2\pi Ft)\sigma_z$ in the Hamiltonian where F is the microwave frequency and ε_{mw} is the energy-modulation amplitude proportional to the microwave amplitude. This dynamic evolution is similar to that of spins in magnetic resonance. When the MW frequency equals the energy difference of the qubit, the qubit oscillates between the ground state and the excited state. This phenomenon is known as Rabi oscillation. The Rabi frequency depends linearly on the MW amplitude (12–14).

Readout is performed with an underdamped superconducting quantum interference device (SQUID) with a hysteretic current-voltage characteristic in direct contact with the qubit loop (Fig. 1A). The mutual coupling M is relatively large because of the shared kinetic and geometric inductances of the joint part enhancing the qubit signal. After performing the qubit operation, a bias current pulse I_b is applied to the SQUID (15). The I_b pulse consists of a short current pulse of length $\sim$50 ns followed by a trailing plateau of $\sim$500 ns (Fig. 1B). During the current pulse, the SQUID either switches to the gap voltage or stays at zero voltage. The pulse height and length are set to optimize the distinction of the switching probability between the two qubit states, which couple to the SQUID through the associated circulating currents. Because the readout electronics has a limited bandwidth of $\sim$100 kHz, a voltage pulse of 50 ns is too short to be detected. For that reason the trailing plateau is added, with a current just above the retrapping current of the SQUID. The whole shape is adjusted for maximum readout fidelity. The switching probability is obtained by repeating the whole sequence of reequilibration, microwave control pulses, and readout typically 5000 times.

When the SQUID bias current is switched on, the circulating current in the SQUID changes. This circulating current, coupled to the qubit through the mutual inductance, changes the phase bias of the qubit by an estimated amount 0.01π. Consequently, the phase bias at which the quantum operations are performed is different from the phase bias at readout. This can be very useful because at the phase bias near π, where the qubit is least sensitive to flux noise, the expectation

values for the qubit circulating current are extremely small. The automatic phase bias shift can be used to operate near π and to perform readout at a bias with a good qubit signal (11). Care must be taken that the fast shift remains adiabatic and that the whole sequence is completed within the relaxation time.

The average SQUID switching current I_{sw} versus applied flux shows the change of the qubit ground-state circulating current (Fig. 2B). Here, the I_b pulse amplitude is adjusted such that the averaged switching probability is maintained at 50%. A step corresponding to the change of qubit circulating current was observed (around the dashed line). The relative variation of 2.5% of I_{sw} is in agreement with the estimation based on the qubit current I_p and the qubit-SQUID mutual inductance M.
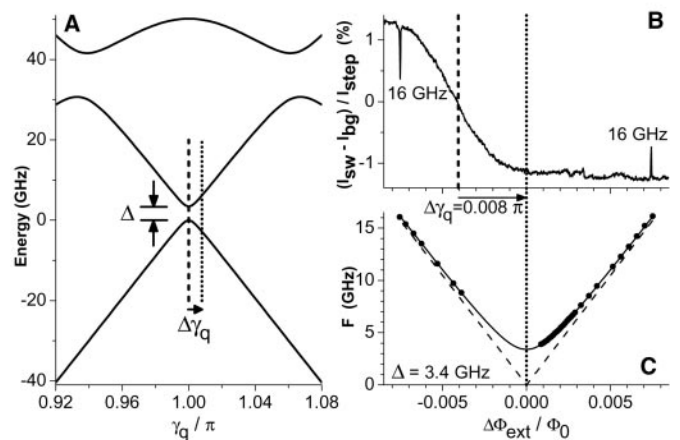
The relevant two energy levels of the qubit were first examined by spectroscopic means. Before each readout, a long microwave pulse (1 μs) at a series of frequencies was applied to observe resonant absorption peaks/dips each time the qubit energy separation E_{10}—adjusted by changing the external flux—coincides with the MW frequency F (10). The dots in Fig. 2C are measured peak/dip positions, obtained by varying F, whereas the continuous line is a numerical fit produced by exact diagonalization (compare Fig. 2A) giving an energy gap $\Delta \approx 3.4$ GHz. The curves in Fig. 2, B and C, are plotted against the change $\Delta\Phi_{ext}$ in external flux from the symmetry position indicated by the dotted line. In agreement with our numerical simulations, the step (Fig. 2B) is shifted away from the symmetry position of the energy spectrum (Fig. 2C) by a phase bias shift $\Delta\gamma_q \approx 2\pi(\Delta\Phi_{ext}/\Phi_0) \approx 0.008\pi$. The step reflects the external-flux dependence of the qubit circulating current at $I_b \approx I_{sw}$ (after the shift), whereas the spectrum reflects E_{01} at $I_b = 0$ (before the shift) (16).

Next, we used different MW pulse sequences to induce coherent quantum dynamics of the qubit in the time domain. For a given level separation E_{10}, a short resonant MW pulse of variable length with frequency $F = E_{10}$ was applied. Together with the MW amplitude, the pulse length defines the relative occupancy of the ground state and the excited state. The corresponding switching probability was measured with a fixed-bias current pulse amplitude. We obtained coherent Rabi oscillations of the qubit circulating current for a frequency $F = 6.6$ GHz and three different values of the MW power A (Fig. 3). The variation in switching probability is around 60%, indicating that the fidelity in a single readout is of that order. By varying A, we verified the linear dependence of the Rabi frequency on the MW amplitude, a key signature of the Rabi process (Fig. 3B). The oscillation pattern can be fitted to a damped sinusoid. For relatively strong driving (Rabi period below 10 ns), decay times τ_{Rabi} up to $\sim$150 ns are obtained. This large decay time resulted in hundreds of coherent oscillations at large microwave power.

The Rabi scheme also allows the study of the state occupancy relaxation. This can be done by applying a coherent π pulse for full rotation of the qubit into the excited state and varying the delay time before readout. Experiments performed at $F = 5.71$ GHz gave an exponential decay with relaxation time $\tau_{relax} \approx 900$ ns.

As a next step we measured the undriven, free-evolution dephasing time τ_φ by performing a Ramsey interference experiment (17) as follows. Two $\pi/2$ pulses, whose length is determined from the Rabi precession presented above, are applied to the qubit. The first pulse creates a superposition of the $|0\rangle$ and $|1\rangle$ states. If the microwave frequency is detuned by $\delta F = E_{10} - F$ away from resonance, the superposition phase increases with a rate

Fig. 2. (**A**) Calculated energy diagram for the three-junction qubit, for $E_J/E_C = 35$, $E_C = 7.4$ GHz, and $\alpha = 0.8$ (11). $\Delta\gamma_q$ indicates the phase shift induced by the SQUID bias current. (**B**) Ground-state transition step: The sinusoidal background modulation of the SQUID (I_{bg}) is subtracted from the I_b pulse amplitude corresponding to 50% switching probability (I_{sw}) and then normalized to I_{step}, the middle value (at the dashed line). A sharp peak and dip are induced by a long (1 μs) MW radiation burst at 16 GHz, allowing the symmetry point to be found (midpoint of the peak/dip positions, dotted line). Data show I_{sw} versus $\Delta\Phi_{ext}$, the deviation in external flux from this point. The transition step is displaced from this point by $\Delta\gamma_q/2\pi$. (**C**) Frequency of the resonant peaks/dips (dots) versus $\Delta\Phi_{ext}$; the continuous line is a numerical fit with the same parameters as in (A) leading to a value of $\Delta = 3.4$ GHz, whereas the dashed line depicts the case $\Delta = 0$.

$2\pi\delta F$, in the frame rotating with the MW frequency F. After a varying delay time, we apply another $\pi/2$ pulse to measure the final $|0\rangle$ and $|1\rangle$ state occupancy via the switching probability. The readout shows Ramsey fringes with a period $1/\delta F$, as in Fig. 4A, where $E_{10} = 5.71$ GHz and $\delta F = 220$ MHz. The dots represent experimental data, whereas the continuous line is an exponentially damped sinusoidal fitting curve, yielding a free-evolution dephasing time $\tau_\varphi \approx 20$ ns. Note that the oscillation period of 4.5 ns agrees well with $1/\delta F$.

Additional information on the spectral properties of the decohering fluctuations can be obtained with a modified Ramsey experiment. By inserting a π pulse between the two $\pi/2$ pulses (Fig. 4B), we obtain a spin-echo pulse configuration. The role of the π pulse is to reverse the noise-driven diffusion of the qubit phase at the midpoint in time of the free evolution. Dephasing due to fluctuations of lower frequencies should be cancelled by their opposite influence before and after the π pulse (18). Spin-echo oscillations (Fig. 4B) are taken under the same conditions as the Ramsey fringes, but are here recorded as a

function of the π pulse position. The period ($\sim$2.3 ns) is half that of the Ramsey interference. We measured the decay of the maximum spin-echo signal (i.e., with the π pulse in the center) versus the delay time between the two $\pi/2$ pulses. The data can be fitted to a half-Gaussian (not shown) with a decay time $\tau_{\text{echo}} \approx 30$ ns.

We conclude that with the present device and setup, the dephasing time $\tau_\varphi \approx 20$ ns, as measured with the Ramsey pulses, is much shorter than the relaxation time $\tau_{\text{relax}} \approx 900$ ns. Dephasing is probably caused by a variation in time of the qubit energy splitting, attributable to external or internal noise. A likely source is external flux noise, which can be reduced in the future. The present qubit could not be operated at the symmetry point $\gamma_q = \pi$ where the influence of flux noise is minimal (5), presumably as the result of an accidentally close SQUID resonance (19). Other possible noise sources are thermal, charge, critical current, and spin fluctuations. From estimations of the Johnson noise in the bias circuit (20, 21), we find a contribution that is several orders of magnitude weaker.

For strong driving, Rabi oscillations persisted for times much longer than τ_φ. This

constitutes no inconsistency. The dependence of the Rabi period on the detuning, due to fluctuations of the qubit energy E_{10}, is weak when the Rabi period is short. The fact that coherence is only marginally improved by the π pulse in the spin-echo experiment seems to indicate the presence of noise at frequencies beyond 10 MHz. Further analysis and additional measurements are needed.

These first results on the coherent time evolution of a flux qubit are very promising. The already high fidelity of qubit excitation and readout can no doubt be improved. Quite likely it is also possible to reduce the dephasing rate. Taken together, these results establish the superconducting flux qubit as an attractive candidate for solid-state quantum computing.

References and Notes
1. A. J. Leggett, A. Garg, *Phys. Rev. Lett.* **54**, 857 (1985).
2. M. A. Nielsen, I. L. Chuang, *Quantum Computation and Quantum Information* (Cambridge Univ. Press, Cambridge, 2000).
3. Y. Makhlin *et al.*, *Rev. Mod. Phys.* **73**, 357 (2001).
4. Y. Nakamura *et al.*, *Nature* **398**, 786 (1999).
5. D. Vion *et al.*, *Science* **296**, 886 (2002).
6. Y. Yu *et al.*, *Science* **296**, 889 (2002).
7. J. M. Martinis *et al.*, *Phys. Rev. Lett.* **89**, 117901 (2002).
8. J. E. Mooij *et al.*, *Science* **285**, 1036 (1999).
9. J. R. Friedman *et al.*, *Nature* **406**, 43 (2000).
10. C. H. van der Wal *et al.*, *Science* **290**, 773 (2000).
11. The two opposite persistent current states, depicted by arrows in Fig. 1A, describe the basis $\{|\uparrow\rangle, |\downarrow\rangle\}$ of Pauli spin matrices. Using the notation $\tan 2\theta = \Delta/\varepsilon$, the qubit eigenstates can be written as $|0\rangle = \cos\theta|\uparrow\rangle + \sin\theta|\downarrow\rangle$ and $|1\rangle = -\sin\theta|\uparrow\rangle + \cos\theta|\downarrow\rangle$ and the expectation values of the corresponding circulating currents as $I_{q0,1} = \pm I_p \cos 2\theta$.
12. I. I. Rabi, *Phys. Rev.* **51**, 652 (1937).
13. M. Grifoni, P. Hänggi, *Phys. Rep.* **304**, 229 (1998).
14. In the frame rotating at the MW frequency $F = E_{10}$, the Rabi precession is around the x axis with a frequency $(\varepsilon_{\text{mw}} \sin 2\theta)/h$ [with θ as in (11)].
15. During the qubit initialization and control, the SQUID bias current is set to zero and, as a result of the SQUID symmetry, the qubit is decoupled from the external current noise to first order. At $I_b = 0$, small external noise current flows equally in the two branches of the SQUID even in the presence of the circulating current in the SQUID. See also (21).
16. A part of the energy spectrum is missing, because the readout is not efficient around the step and thus the spectroscopy signal is weak.
17. N. F. Ramsey, *Phys. Rev.* **78**, 695 (1950).
18. E. L. Hahn, *Phys. Rev.* **80**, 580 (1950).
19. In the present device, $\Delta \approx 3.4$ GHz was rather close to the SQUID plasma frequency designed to be $\sim$2 GHz (at $I_b \approx I_{\text{sw}}$). This could be a possible explanation for the absence of coherent oscillations for $F = \Delta$.
20. Lin Tian, S. Lloyd, T. P. Orlando, *Phys. Rev. B* **65**, 144516 (2002).
21. C. H. van der Wal, F. K. Wilhelm, C. J. P. M. Harmans, J. E. Mooij, *Eur. Phys. J. B* **31**, 111 (2003).
22. We thank R. N. Schouten, J. B. Majer, A. Lupascu, and K. Semba for experimental help and discussion; D. Esteve and C. Urbina for valuable input; and D. Vion, A. Aassime, C. H. van der Wal, A. C. J. ter Haar, T. Orlando, S. Lloyd, M. Grifoni, F. K. Wilhelm, L. Vandersypen, and P. C. E. Stamp for fruitful discussions. Supported by the Dutch Foundation for Fundamental Research on Matter (FOM), the European Union SQUBIT project, and the U.S. Army Research Office (grant DAAD 19-00-1-0548).

Fig. 3. (A) Rabi oscillations for a resonant frequency $F = E_{10} = 6.6$ GHz and three different microwave powers $A = 0$, -6, and -12 dBm, where A is the nominal microwave power applied at room temperature. The data are well fitted by exponentially damped sinusoidal oscillations. The resulting decay time is $\sim$150 ns for all powers. **(B)** Linear dependence of the Rabi frequency on the microwave amplitude, expressed as $10^{A/20}$. The slope is in agreement with estimations based on sample design.
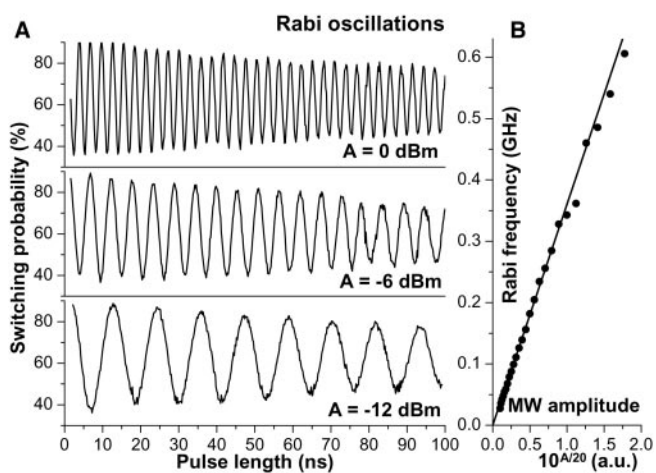

Fig. 4. (A) Ramsey interference: The measured switching probability (dots) is plotted against the time between the two $\pi/2$ pulses. The continuous line is a fit by exponentially damped oscillations with a decay time of 20 ns. The Ramsey interference period of 4.5 ns agrees with the inverse of the detuning from resonance, 220 MHz. The resonant frequency is 5.71 GHz and microwave power $A = 0$ dBm. **(B)** Spin-echo experiment: switching probability versus position of the π pulse between two $\pi/2$ pulses. The period of $\sim$2.3 ns corresponds well to half the inverse of the detuning. The width and timing of microwave pulses in the MW line are shown in each graph. The readout pulse in the bias line immediately follows the last $\pi/2$ pulse (see Fig. 1B).